

# The radii of M-dwarfs in the young open cluster NGC 2516

R.J. Jackson, R.D. Jeffries and P.F.L. Maxted

*Astrophysics Group, Research Institute for the Environment, Physical Sciences and Applied Mathematics, Keele University, Keele, Staffordshire ST5 5BG*

Submitted July 1 2009

## ABSTRACT

Using a novel technique, which combines previously determined rotation periods with new spectroscopic determinations of projected rotation velocity, we have determined radii for fast rotating, low-mass ( $0.2\text{--}0.7 M_{\odot}$ ) M-dwarfs in the young, solar-metallicity open cluster, NGC 2516. The mean radii are larger than model predictions at a given absolute  $I$  or  $K$  magnitude and also larger than the measured radii of magnetically inactive M-dwarfs; the difference increases from a few per cent, to 50 per cent for the lowest luminosity stars in our sample. We show that a simple two-temperature starspot model is broadly capable of explaining these observations, but requires spot coverage fractions of about 50 per cent in rapidly rotating M-dwarfs.

**Key words:** stars: fundamental parameters – stars: spots – clusters and associations: NGC2516.

## 1 INTRODUCTION

The radius of a star is among the most fundamental properties that can be predicted by a stellar model. Yet recent measurements of radii for K- and M-dwarfs in eclipsing binary systems reveal significant discrepancies between models and observations. For a given mass, the radii of stars with  $0.3 < M/M_{\odot} < 0.8$  are up to 20 per cent larger than predicted by evolutionary models, and so the effective temperature at a given luminosity is over-predicted by up to 10 per cent (López-Morales 2007; Morales et al. 2009). Attempts to explain these discrepancies have focused on the role of magnetic fields in suppressing convection and producing cool starspots (D’Antona et al. 2000; Mullan et al. 2001; Chabrier, Gallardo & Baraffe 2007). Strong, dynamo-generated magnetic fields are expected in the tidally locked, rapidly rotating components of eclipsing binaries, but if these effects are important they should also cause larger radii for active, single stars. Confirming this is challenging because (i) the small number of low-mass stars close enough to measure precise interferometric radii are magnetically inactive, and (ii) metallicity variations, which are difficult to accurately assess in cool field dwarfs, could be a significant source of radius scatter (Berger et al. 2006).

In this letter we present radius estimates for rapidly rotating, and hence magnetically active, single, cool dwarfs in the young, open cluster NGC 2516, which has a close-to-solar metallicity. Our novel, purely geometric technique uses spectroscopic measurements of projected equatorial velocities along with rotation periods from light curve modulation to infer projected stellar radii. Our targets have masses  $0.2 < M/M_{\odot} < 0.7$ , covering spectral types M0–M5, reach-

ing masses at which stars are expected to be fully convective. We show that, like the low-mass components of eclipsing binaries, these stars have significantly larger radii than model predictions and that widespread coverage with dark, magnetic starspots is a plausible explanation.

## 2 OBSERVATIONS OF NGC 2516

NGC 2516 is a young open cluster with a large population of low-mass stars (Hawley, Tourtellot & Reid 1999; Jeffries, Thurston & Hambly 2001). It has a close-to-solar metallicity, spectroscopically determined as  $[\text{Fe}/\text{H}] = 0.01 \pm 0.07$  or photometrically as  $[\text{M}/\text{H}] = -0.05 \pm 0.14$  (Terndrup et al. 2002). The same authors give an intrinsic distance modulus of  $7.93 \pm 0.14$  based on main sequence fitting. The cluster age is  $\simeq 150$  Myr based on the nuclear turn-off in its high-mass stars and the lithium depletion and X-ray activity seen in cooler stars (Jeffries, James & Thurston 1998; Lyra et al. 2006). The cluster reddening is  $E(B - V) = 0.12 \pm 0.02$  (Terndrup et al. 2002).

Targets in NGC 2516 were observed using the VLT (UT-2 Kueyen) FLAMES instrument feeding the GIRAFFE and UVES fibre spectrographs. Primary targets were chosen from 362 candidate cluster members reported by Irwin et al. (2007), that have measured rotation periods in the range 0.1–15 days and  $14.5 < I < 18.5$ , corresponding approximately to  $0.2 < M/M_{\odot} < 0.7$  (Baraffe et al. 2002). Spare fibres were placed on “blank” sky positions and on other photometric candidates for which no rotation periods were known. The GIRAFFE spectrograph was used with the HR20A grating, covering the wavelength range 8000–8600 Å

at a resolving power of 16 000. Bright blue stars in the same field were used for telluric compensation and observed simultaneously using UVES. Eight observation blocks (OBs) were recorded in service mode between 27 November and 30 December 2007. Each OB consisted of two 1280 s exposures with GIRAFFE and three 800 s UVES exposures. One of the OBs was performed twice sequentially with no change in instrument setup. Some targets were also observed in multiple OBs. A total of 867 spectra were recorded of 678 unique targets.

## 2.1 Extraction of the target spectra

Many of the spectra were faint, requiring optimal extraction to provide sufficient signal-to-noise ratio (SNR) for useful analysis. There was also significant telluric absorption and strong sky emission lines in the spectra. For these reasons we used purpose-built software for data reduction rather than pipelines supplied by the European Southern Observatory.

The method used for optimal extraction is described by Horne (1986). This applies non-uniform weight to pixels in the extraction sum, minimising statistical noise whilst preserving photometric accuracy. In our case, weighting profiles were determined from a boxcar average along the wavelength axis of tungsten-lamp flat field images. Wavelength calibration was based on thorium-argon lamp spectra recorded during the day. Fine offsets were applied to the calibration of individual fibres to compensate for any drift with time. These offsets were determined by comparing the positions of emission lines in the median sky spectra of each OB to their position in sky spectra averaged over all OBs. The offset per fibre varied between 0.001 Å and 0.008 Å. To deal with variations in fibre efficiency, the proportion of the median sky spectrum subtracted from each target spectrum was tuned to minimise the peak amplitude of the cross-correlation between the sky-subtracted target spectrum and the median sky spectrum. Spectra from each OB were averaged and corrected for telluric absorption using the co-temporal UVES spectra of bright blue stars, which were broadened to mimic the GIRAFFE spectral resolution.

## 2.2 Measurement of radial and projected equatorial velocities

Heliocentric radial velocities (RVs) were measured by cross-correlation with stars from the UVES atlas (Bagnulo et al. 2003). Templates of type K4.5V (HD 209100) and M6V (HD 34055) were used. Projected rotation velocities ( $v \sin i$ , where  $i$  is an unknown inclination) were estimated from the cross-correlation function widths. Translation from these to  $v \sin i$  was calibrated by artificially broadening standard star spectra. This was done in two stages. The standards were broadened with a Gaussian to match the cross-correlation function widths to the average width obtained from 40 slow-rotating targets (period,  $P > 5$  days), which we expect to have negligible  $v \sin i$  (compared with the spectral resolution). These broadened spectra were then convolved with a rotational broadening kernel at many  $v \sin i$  values. A linear limb darkening coefficient of 0.6 was used (Claret, Diaz-Cordoves & Gimenez 1995), but our results are quite insensitive to this parameter. The  $v \sin i$  values found using the

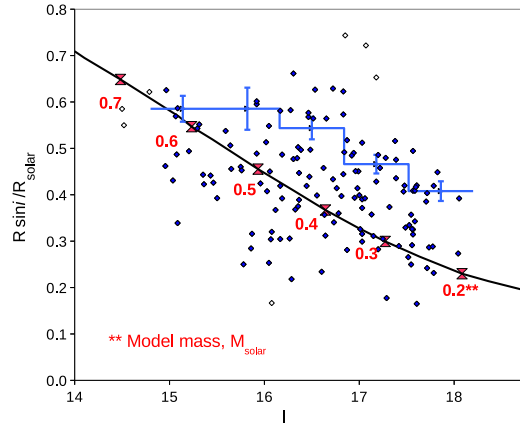


**Figure 1.** Measured radii of stars in NGC 2516 as a function of  $I$ -magnitude. Diamonds show the projected radii ( $R \sin i$ ), solid diamonds were used to determine the average radii. The histogram shows the average radius determined from the mean  $R \sin i$  in each bin. The solid curve is a 158 Myr, solar metallicity isochrone from the Baraffe et al. (2002) models.

two templates did not differ significantly, either on average or as a function of colour, so we adopted the average value.

Uncertainties in RV and the width of the cross-correlation function were measured empirically. Uncertainties due to noise in the target spectra were estimated, as a function of SNR, by comparing results for the two sequential OBs. A constant representing other error sources was determined by comparing observations of the same targets through different fibres in different OBs. Typical RV uncertainties were 0.2–0.6  $\text{km s}^{-1}$  and the normalised uncertainty in  $v \sin i$  was typically  $\simeq 10$  per cent for  $v \sin i > 20 \text{ km s}^{-1}$  but larger for smaller  $v \sin i$ .

## 3 AVERAGE RADII OF CLUSTER MEMBERS

The NGC 2516 photometric candidates used for the radius estimates have  $v \sin i > 8 \text{ km s}^{-1}$ , and most have periods  $< 3$  days (see below). This sample is unlikely to contain many field stars, because fast rotators are rare among the general late-K to mid-M-dwarf field population (Delfosse et al. 1998). Nevertheless, some candidates might be tidally locked binaries seen at an unfortunate phase or have low quality measurements of  $v \sin i$ . To avoid contamination of the sample we excluded: stars with spectra of average SNR less than 5; targets with cross-correlation functions with no clear single peak, or multiple peaks characteristic of a binary pair; stars with measured  $v \sin i$  less than  $8 \text{ km s}^{-1}$  or less than twice their uncertainty. Stars were also excluded with RV more than  $2(\sigma_v^2 + \sigma_c^2)^{1/2}$  from the mean ensemble RV (for all the included stars with measured  $v \sin i$ ), where  $\sigma_v$  is the individual RV uncertainty and  $\sigma_c$  is the intrinsic cluster RV dispersion, determined to be  $\sigma_c = 0.66 \pm 0.13 \text{ km s}^{-1}$ . The latter step was performed iteratively.

The remaining 147 targets were used to determine projected radii using the formula  $R \sin i / R_\odot = 0.124 (P/2\pi) v \sin i$ , where  $P$  is in days and  $v \sin i$  is in  $\text{km s}^{-1}$ . Figure 1 shows projected radii as a function of  $I$ -magnitude. The photometry comes from Irwin et al. (2007),

with a small correction ( $\Delta I = 0.080 - 0.0076 I$  mag) added, to put Irwin et al.'s magnitudes onto the better-calibrated photometric scale established by Jeffries et al. (2001) for low-mass stars in NGC 2516.

Assuming stellar spin axes are randomly orientated, then the mean value of  $R \sin i$  measured over a small range of  $I$ -magnitudes can be divided by the average value of  $\sin i$  to determine the mean radius. A complication is that it is not possible to measure the period of stars, or determine  $v \sin i$  values if they are viewed at small inclination angles, resulting in an upward bias in the mean  $\sin i$  (see Jeffries 2007). If we consider a cut-off inclination,  $\tau$ , such that stars with  $\sin i < \tau$  yield no period or  $R \sin i$  value, then the normalised probability density of  $i$  becomes

$$P(i) = \sin i / \cos(\arcsin \tau) \quad \text{for } \tau < \sin i < 1, \quad (1)$$

and the mean value of  $\sin i$  becomes

$$\int \sin i P(i) di = \tau/2 + (\pi/2 - \arcsin \tau)/2 \cos(\arcsin \tau). \quad (2)$$

Equation 2 can be used to determine the mean radius from a set of  $R \sin i$  values providing  $\tau$  is known. Here  $\tau$  is estimated by forming a cumulative distribution of the measured values of  $R \sin i$  normalized with a regression line against  $I$  magnitude. This is compared with the cumulative distribution predicted (by Monte Carlo simulation) from the product of the modified  $\sin i$  distribution of equation 1 and a normal distribution representing the measurement uncertainties in  $R \sin i$ , which is dominated by the error in  $v \sin i$ . A Kolmogorov-Smirnov test is used to compare the measured and predicted distributions for various  $\tau$  values, yielding a best-fit  $\tau = 0.40^{+0.06}_{-0.08}$ , and hence an average value of  $\sin i$  of  $0.832^{+0.015}_{-0.013}$  from equation 2. This compares with a value of 0.785 if this effect were neglected, showing that it is a small correction with an even smaller uncertainty when compared with the size of the effects we will subsequently discuss.

### 3.1 Variation of radius with $I$ magnitude

Figure 1 shows individual  $R \sin i$  measurements and the average radius estimated in five equally spaced bins for  $14.8 < I < 18.2$ . Uncertainties in the binned mean radii are the quadrature sum of uncertainties in the average  $R \sin i$  and uncertainty in the mean  $\sin i$ . A few stars were excluded from the binning process (but are still shown in Fig. 1), because they either fell outside these magnitude ranges, or were more than 2 standard deviations away from the regression line between  $R \sin i$  and  $I$  discussed in the last subsection. Several of the latter have long periods  $> 4$  days and may have incorrect periods at a 1-day alias of the correct period (see Irwin et al. 2007), or over-estimated  $v \sin i$  because of unresolved binarity (see below).

Also shown in Fig. 1 is a solar metallicity 158 Myr isochrone from the Baraffe et al. (2002) models, which use a convective mixing length of 1 pressure scale height. The absolute  $I$  magnitudes of the isochrones were shifted according to a distance modulus ( $7.93 \pm 0.14$  – Terndrup et al. 2002) and extinction ( $A_I = 1.78 E(B - V) = 0.213$  mag), with a net uncertainty of about  $\pm 0.15$  mag. From this diagram it appears that the cool stars observed in NGC 2516 have larger radii (at a given  $I$ ) than predicted by the models, by

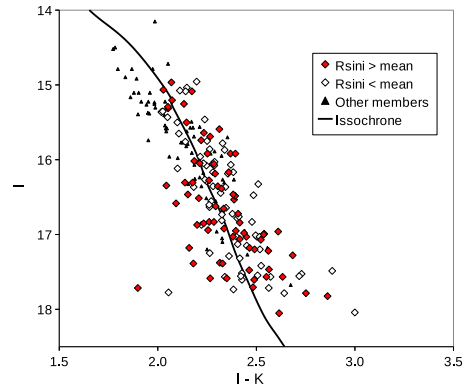


**Figure 2.** A colour magnitude diagram for targets in NGC 2516. Solid diamonds show members with  $R \sin i$  above the mean of their bin, open diamonds show  $R \sin i$  below. Triangles are members with no  $R \sin i$  measurement. The line is a 158 Myr solar metallicity isochrone (Baraffe et al. 2002).

a factor increasing from a few per cent at  $I \simeq 15$  (corresponding to  $M \simeq 0.6 M_{\odot}$ ), to about 50 per cent at  $I \simeq 18$  ( $M \simeq 0.2 M_{\odot}$ ). A plot can be constructed for  $R \sin i$  versus  $K$  magnitude and a similar discrepancy between observed and predicted radii is present.

### 3.2 Colour magnitude diagram

The cluster may contain spectrally unresolved binary systems that are seen at a phase/velocity-separation that results in them having the cluster RV, but an over-estimated  $v \sin i$  and hence over-estimated  $R \sin i$ . Conversely, unresolved binaries will be shifted by up to 0.75 mag leftward in Fig. 1, which would artificially reduce the discrepancy between observed radii and models.

To check this, Fig. 2 shows the  $I$  vs  $I - K$  colour magnitude diagram (CMD) for all target stars with  $\text{SNR} > 5$ , where we identify stars with  $R \sin i$  above or below the mean of their bins in Fig. 1.  $K$  magnitudes from the 2MASS catalog (Cutri et al. 2003) are transformed to the CIT system using the correction ( $K_{\text{CIT}} = K_{2\text{MASS}} + 0.024$ ) given by Carpenter (2001). Compared to a 158 Myr isochrone from Baraffe et al. (2002), both classes of object lie redward by an average of 0.06 mag and are statistically indistinguishable. Because we know that binaries where both components contribute to the magnitude and observed spectrum should be shifted up and to the right in this CMD, we can say that the  $R \sin i$  distribution appears unaffected by binarity.

## 4 DISCUSSION

Figure 3 shows the mean radii for our NGC 2516 sample, binned as a function of absolute  $I$  and intrinsic  $I - K$ , compared with various isochrones (from Baraffe et al. 2002, with a mixing length of 1 pressure scale height) and with data for single field stars. Interferometric radii and parallaxes for these stars are from Demory et al. (2009),  $I$  magnitudes are from Leggett (1992) and  $K$  magnitudes are from 2MASS, converted to the CIT system. The field stars have low magnetic activity levels as judged from their coronal X-ray emis-

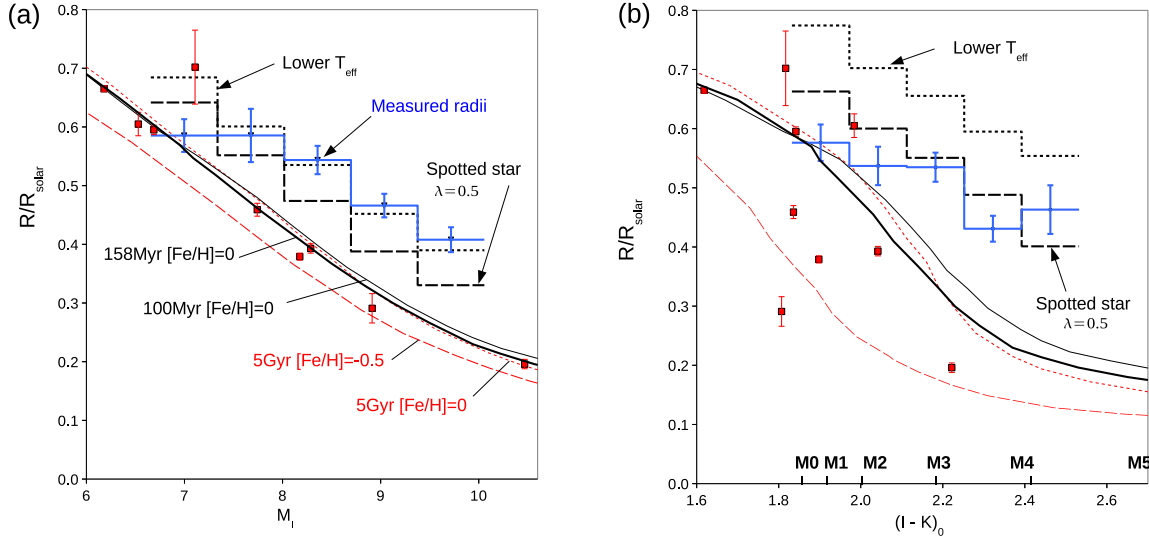


**Figure 3.** Comparison of measured radii with model isochrones as a function of absolute  $I$  and intrinsic  $I - K$ . The solid histogram shows the mean value and expected uncertainty of measured radii in NGC2516. Squares show directly measured radii for field stars. The labelled lines shows model isochrones for various ages and metallicities from Baraffe et al. 2002. The dotted and dashed histograms show the expected radius for (i) stars with a uniformly lower  $T_{\text{eff}}$  and (ii) heavily spotted stars with 50 per cent spot coverage.

sion, but a range of metallicities (López-Morales 2007). The 5 Gyr isochrone for solar metallicity stars is in reasonable agreement with the radii of inactive field stars (Demory et al. 2009). Comparison of the measured and predicted radii as a function of  $I - K$  shows more scatter, but the majority of this scatter can be interpreted as a metallicity effect. The 5 Gyr isochrone for  $[\text{Fe}/\text{H}]=-0.5$  in Fig. 3b, shows that metallicity strongly affects  $I - K$ , since, at a given radius, the  $I$  magnitude is more sensitive to metallicity than  $K$ .

Turning now to NGC 2516, the metallicity complication is not present – we know it has a close-to-solar metallicity (Terndrup et al. 2002). The mean radii (as a function of  $I$ ,  $K$  or  $I - K$ ) show an increasing departure from the 158 Myr solar metallicity isochrone with decreasing luminosity and increasing colour (decreasing  $T_{\text{eff}}$ ). Even reducing the assumed cluster age to 100 Myr (a fairly firm lower limit), does little to mitigate the discrepancy (see Fig. 3). Uncertainties in the assumed extinction and reddening produce the equivalent of only  $\pm 3$  per cent systematic error in the observed radii and the distance uncertainty is limited to shifting the models in Fig. 3a by  $\pm 0.14$  mag along the x-axis. We conclude that the radii of low-mass stars in NGC 2516 do show departures from model predictions and from the observed radii of inactive stars. The radius discrepancies grow as we move to lower luminosities and mass, becoming as much as 50 per cent larger at  $M_I \simeq 10$ ,  $M_K \simeq 7.5$ , corresponding to  $M \simeq 0.2 M_{\odot}$  in the Baraffe et al. (2002) models.

Direct comparison with other models of stellar evolution is more difficult since these use empirical bolometric corrections to convert  $T_{\text{eff}}$ /luminosity to predicted colour/magnitudes. However, the low-mass models of D’Antona & Mazzitelli (1997) and Siess, Dufour & Forestini (2000) predict similar or even slightly smaller radii for a given luminosity than Baraffe et al. (2002), so the discrepancy does not just exist for this latter set of models.

#### 4.1 Effect of spot coverage

The measured radii of the cool NGC 2516 stars are significantly higher than predicted by evolutionary models. Similar discrepancies as large as 20–30 per cent are reported for active stars in binary systems (López-Morales 2007). Chabrier et al. (2007) discussed two possible causes for this observed increase in radius. The first was a change in mixing length in magnetically active stars affecting heat transfer. The second was high levels of magnetic starspot coverage. They showed that reductions in mixing length had only small effects for fully convective stars where convection is nearly adiabatic. Here we find larger radius anomalies for the cooler, fully convective stars, leading us to consider surface spotting.

The NGC 2516 stars with measured  $R \sin i$  have median rotation periods of 0.76 days, with 95 per cent less than 3 days. In either single or binary M-dwarfs, this rotation should lead to saturated levels of magnetic activity (e.g. James et al. 2000). Cross-correlating our sample with the NGC 2516 targets in Hawley et al. (1999), we find 27 matches. Of these, 11 stars have measured periods and  $R \sin i$  values. All 11 show  $H\alpha$  in emission effectively defining the upper envelope of magnetic activity in the cluster.

To quantify spot coverage effects, a simple model assuming a fixed luminosity is used to predict changes in magnitude and colour with spot temperature and area. We start from the assumption that the Baraffe et al. (2002) models do a reasonable job in predicting the radii, temperature and  $I - K$  of inactive and presumably unspotted stars (see Fig. 3 and the discussion in Baraffe et al. 1998). If the surface temperature of the star is reduced from  $T_0$  to  $T$  then to maintain a fixed luminosity the radius increases as  $R = R_0(T_0/T)^{1/2}$ . Whilst this does not effect the bolometric magnitude, it does affect  $M_I$  and  $M_K$ , since the bolometric corrections,  $BC_I$  and  $BC_K$ , are functions of  $T$  and  $R$ . Changes in  $BC_I$  and  $BC_K$  with  $T$  are found from the 158 Myr isochrone. The second order effect due to larger  $R$  (and hence lower surface

gravity) is estimated by interpolating model isochrones for M-dwarfs from 15.8 to 158 Myr. Bolometric corrections at  $T$  are used to determine modified isochrones and hence  $M_I$  and  $M_K$  for a star at the spot temperature. A fraction  $\lambda$ , of this star is combined with a fraction  $(1 - \lambda)$  of an unspotted star of similar radius to determine the magnitude and colour of the spotted star as a function of radius.

Two dashed histograms in Fig. 3 present results for representative experiments. Calculated radii at the measured  $M_I$  and  $(I - K)_0$  are binned to compare with the measurements. The first model shows the result of a uniform 15 per cent temperature reduction in the models (i.e.  $\lambda = 1$ ). This provides a reasonable match for radius vs  $M_I$ , but fails to predict the correct stellar colours in Fig. 3b, because the temperature dependence of  $BC_K$  is very different to that of  $BC_I$ . Instead we simulate the radii of heavily spotted stars with  $\lambda = 0.5$  and spots that are 30 per cent cooler than the unspotted photosphere; at the upper end of spectroscopically deduced spot coverages for active stars (e.g. O'Neal et al. 2004). The match between predicted and measured radii is much improved in the radius vs  $M_I$  plot *and* the radius vs  $(I - K)_0$  plot. Even better agreement to the lower luminosity bins can be achieved using  $\lambda \simeq 0.75$  and 45 per cent spot temperature reductions. Such high filling factors are suggested by investigations of Zeeman broadening due to magnetic fields in rapidly rotating M-dwarfs (e.g. Johns-Krull & Valenti 2000; Reiners, Basri & Browning 2009) However, this level of precision is probably over-interpretation at this stage. The remaining discrepancies could also be due to uncertainties in the cluster metallicity or inaccuracies in the unspotted model isochrone of radius versus  $(I - K)_0$ .

## 5 SUMMARY

The results reported here show that the radii of young, single, rapidly rotating M-dwarfs in NGC 2516 are significantly larger, at a given luminosity, than predicted by evolutionary models and hence their effective temperatures must be cooler than predicted. The discrepancy becomes larger for stars less luminous than the predicted transition to fully convective structures, reaching a radius anomaly of 50 per cent. These results are consistent, although more extreme for the lowest mass stars in our sample, with radius anomalies found for the components of older, tidally locked eclipsing binary systems. Evolutionary models correctly predict the radii of magnetically in-active stars, suggesting that the increased radii in our sample is caused by rapid rotation and/or magnetic activity. A simple, two-temperature starspot model could explain the overall radius increase, but only if spots cover  $\geq 50$  per cent of the surface for the lowest luminosity objects in our sample.

Cool stars may be rapidly rotating and magnetically active as a consequence of their youth or membership of tidally locked binary systems. An altered relationship between mass, radius and effective temperature for these stars calls for improvements in low-mass models in order to interpret observations of young clusters, star forming regions and close binary systems.

## ACKNOWLEDGEMENTS

Based on observations collected at the European Southern Observatory, Paranal, Chile through observing programs 380.D-0479 and 266.D-5655. RJJ acknowledges receipt of an STFC studentship.

## REFERENCES

- Bagnulo, S. et al. 2003, *Messenger*, 114, 10  
 Baraffe I., Chabrier G., Allard F., Hauschildt P. H., 1998, *A&A*, 337, 403  
 Baraffe I., Chabrier G., Allard F., Hauschildt P. H., 2002, *A&A*, 382, 563  
 Berger, D. H. et al. 2006, *ApJ*, 644, 475  
 Carpenter J. M., 2001, *AJ*, 121, 2851  
 Chabrier G., Gallardo J., Baraffe I., 2007, *A&A*, 472, L17  
 Claret A., Diaz-Cordoves J., Gimenez A., 1995, *A&AS*, 114, 247  
 Cutri, R. M. et al. 2003, Technical report, Explanatory supplement to the 2MASS All Sky data release. <http://www.ipac.caltech.edu/2mass/>  
 D'Antona F., Mazzitelli I., 1997, *Memorie della Societa Astronomica Italiana*, 68, 807  
 D'Antona F., Ventura P., Mazzitelli I., 2000, *ApJ*, 543, L77  
 Delfosse X., Forveille T., Perrier C., Mayor M., 1998, *A&A*, 331, 581  
 Demory, B. -O et al. 2009, arXiv:0906.0602  
 Hawley S. L., Tourtellot J. G., Reid I. N., 1999, *AJ*, 117, 1341  
 Horne K., 1986, *PASP*, 98, 609  
 Irwin J., Hodgkin S., Aigrain S., Hebb L., Bouvier J., Clarke C., Moraux E., Bramich D. M., 2007, *MNRAS*, 377, 741  
 James D. J., Jardine M. M., Jeffries R. D., Randich S., Collier Cameron A., Ferreira M., 2000, *MNRAS*, 318, 1217  
 Jeffries R. D., 2007, *MNRAS*, 381, 1169  
 Jeffries R. D., James D. J., Thurstun M. R., 1998, *MNRAS*, 300, 550  
 Jeffries R. D., Thurstun M. R., Hambly N. C., 2001, *A&A*, 375, 863  
 Johns-Krull C. M., Valenti J. A., 2000, in Pallavicini R., Micela G., Sciortino S., eds, *Stellar Clusters and Associations: Convection, Rotation, and Dynamos Vol. 198* of *Astronomical Society of the Pacific Conference Series*. pp 371–+  
 Leggett S. K., 1992, *ApJS*, 82, 351  
 López-Morales M., 2007, *ApJ*, 660, 732  
 Lyra W., Moitinho A., van der Blied N. S., Alves J., 2006, *A&A*, 453, 101  
 Morales, J. C. et al. 2009, *ApJ*, 691, 1400  
 Mullan D. J., MacDonald J., 2001, *ApJ*, 559, 353  
 O'Neal D., Neff J. E., Saar S. H., Cuntz M., 2004, *AJ*, 128, 1802  
 Reiners A., Basri G., Browning M., 2009, *ApJ*, 692, 538  
 Siess L., Dufour E., Forestini M., 2000, *A&A*, 358, 593  
 Terndrup D. M., Pinsonneault M., Jeffries R. D., Ford A., Stauffer J. R., Sills A., 2002, *ApJ*, 576, 950

This paper has been typeset from a  $\text{\TeX}/\text{\LaTeX}$  file prepared by the author.